Inorg. Chem. **2004**, *43*, 4702–4707

Sensing of Sulfur Dioxide by Base Metal Thiolates: Structures and Properties of Molecular NiN_2S_2/SO_2 Adducts

Melissa L. Golden, Jason C. Yarbrough, Joseph H. Reibenspies, and Marcetta Y. Darensbourg*

Texas A&M University, Department of Chemistry, College Station, Texas 77843

Received April 21, 2004

The cis-dithiolate N_2S_2Ni complex bismercaptoethanediazacycloheptanenickel(II), (bme-dach)Ni or **Ni-1′**, takes up two equivalents of sulfur dioxide in which thiolate-sulfur to SO_2-sulfur interactions are well-defined by X-ray crystallography. **Ni-1′**·$2SO_2$, $C_9H_{18}N_2NiO_4S_4$, yields monoclinic crystals belonging to the *P*2(1)/*c* space group: $a = 10.308(4)$ Å, $b = 13.334(5)$ Å, $c = 10.842(4)$ Å, $\alpha = 90°$, $\beta = 91.963(6)°$, $\gamma = 90°$, and $Z = 4$. Further characterization by ν(SO) IR spectroscopy, thermal gravimetric analysis, electronic spectroscopy, and visual color changes upon reversible SO_2 adduct formation establish **Ni-1′** and the analogous bismercaptoethanediazacyclooctane derivative, (bme-daco)Ni, **Ni-1**, to be viable candidates for technical development as chemical sensors of this noxious gas. Visual SO_2 detection limits of **Ni-1** and **Ni-1′** are established at 25 and 100 ppm, respectively. Both the **Ni-1′**·$2SO_2$ adduct and the **Ni-1′** reactant are air stable. In addition, the stability of **Ni-1′**·SO_2 to vacuum and removal of SO_2 by heating make **Ni-1′** a possible storage/controlled release complex for SO_2 gas.

Introduction

Studies of gas uptake by transition metal complexes have uncovered fundamental properties of structure and bonding of far-reaching significance. For example, the binding of SO_2 to Pt^{II}, Ir^{I}, and Rh^{I} as S-bound, pyramidal η^1-SO_2 has emphasized the nucleophilic character of these d^8 metals and the control that donor ligands might have on the stability of such metallo-base→SO_2 adducts.[1,2] As an application, van Koten and co-workers have developed square planar platinum complexes as sensor materials for the repetitive qualitative and quantitative detection of SO_2.[3−5]

Owing to diminished nucleophilicity, nickel(II) analogues of the van Koten platinum complex bind SO_2 much less strongly.[2] Nevertheless, we and others have noted that the presence of thiolate S-donor ligands within nickel(II) and copper(I) coordination spheres may give rise to SO_2 adduct formation at sulfur.[6−8] A series of $Cu^{I}(PR_3)_n(SR')$ ($n = 2$ or 3) derivatives which formed 1:1 SO_2 adducts at the thiolate-S, was patented as an SO_2 gas indicator by Eller and Kubas.[8,9] With the cis-dithiolate nickel complex, bismercaptoethanediazacyclooctanenickel(II), (bme-daco)Ni or **Ni-1**, a dramatic color change accompanied SO_2 binding.[6,7] Isolated crystals of the **Ni-1**·SO_2 adduct were remarkably stable to vacuum, maintaining crystallinity at ca. 0.5 Torr over the course of, at minimum, 12 h. This stability is ascribed to an extended chain structure in which short- and long-range S···SO_2···S interactions exist in the crystals, Figure 1. Yet, in solution a purge of inert gas readily removed the SO_2.

The **Ni-1**·SO_2 adduct described above is sensitive to O_2, according to Scheme 1. Such a sulfate-forming reaction is driven by disulfide formation and is consistent with the known reactivity of **Ni-1** with O_2. The sulfate-forming reaction also occurs with Ir^{I} complexes which characteristically interact with SO_2 and react with O_2.[10] When present simultaneously, O_2 and SO_2 take up two electrons from Ir^{I} resulting in SO_4^{2-} tightly bound to Ir^{III}. It would thus appear that two single electron oxidations of the thiolate sulfurs in nickel dithiolates achieve a similar sulfate formation from

* Author to whom correspondence should be addressed. Tel: (979) 845-5417. Fax: (979) 845-0158. E-mail: marcetta@mail.chem.tamu.edu.

(1) Kubas; G. J. *Inorg. Chem.* **1979**, *18*, 182−187.
(2) Terheijden, J.; van Koten, G.; Mul; W. P.; Stufkens, D. K.; Muller, F.; Stam, C. *Organometallics* **1986**, *5*, 519−525.
(3) Albrecht, M.; Gossage, R. A.; Spek, A. L.; van Koten, G. *Chem. Commun.* **1998**, 1003−1004.
(4) Albrecht, M.; Lutz, M.; Spek, A. L.; van Koten, G. *Nature* **2000**, *406*, 970−974.
(5) Albrecht, M.; Gossage, R. A.; Lutz, M.; Spek, A. L.; van Koten, G. *Chem. Eur. J.* **2000**, *6*, 1431−1445.
(6) Darensbourg, M. Y.; Tuntulani, T.; Reibenspies, J. H. *Inorg. Chem.* **1994**, *33*, 611−613.
(7) Darensbourg, M. Y.; Tuntulani, T.; Reibenspies, J. *Inorg. Chem.* **1995**, *34*, 6287−6294.
(8) Eller, P. G.; Kubas, G. J. *J. Am. Chem. Soc.* **1977**, *99*, 4346−4351.
(9) Eller, P. G.; Kubas, G. J. U.S. Patent 4,152,118, 1979.
(10) Valentine, J.; Valentine, D.; Collman, J. P. *Inorg. Chem.* **1971**, *10*, 219−225.

10.1021/ic049387n CCC: $27.50
Published on Web 06/25/2004

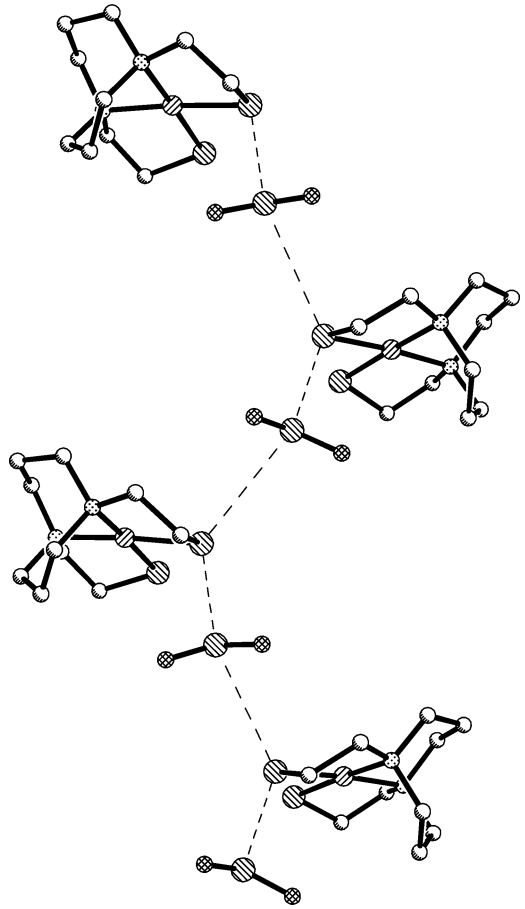

Figure 1. Extended chain interaction of **Ni-1**·SO_2 with a shorter $S_{(thiolate)}\cdots S_{(SO_2)}$ distance of 2.597(2) Å and a second close contact of 3.692(2)Å.[6]

Scheme 1

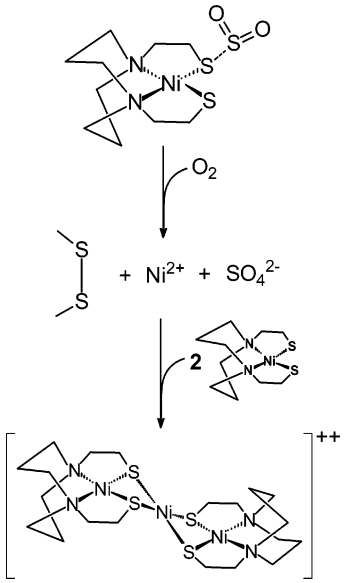

SO_2/O_2 reactants as does the 2-electron oxidation of the single (and expensive) metal, Ir^I. Regardless of this interesting comparison, specificity for SO_2 binding versus O_2 reactivity must be a target for a stable and recyclable gas sensor complex.

Subsequent studies of N_2S_2Ni complexes have focused on a simple modification of the diazacycle framework; i.e., the synthetically challenging daco has been replaced by the commercially available diazacycloheptane, dach.[11] The easily prepared (bme-dach)Ni or **Ni-1′**, displays many similarities to Ni-1; a notable exception is its lack of reactivity with molecular O_2. Yet, as described below, **Ni-1′** readily binds SO_2. The isolation and characterization of the **Ni-1′**·$2SO_2$ and **Ni-1′**·SO_2 adducts and quantification of SO_2 binding abilities in the **Ni-1** and **Ni-1′** complexes is the focus of this report.

Experimental Section

General Procedures. Standard Schlenk techniques were used to avoid exposure to SO_2 gas. (bme-daco)Ni[12] and (bme-dach)Ni[11] were synthesized according to previously reported procedures. Sulfur dioxide gas (99.9+% pure) was purchased from Aldrich Chemical Co. and used as received.

Physical Measurements. UV−vis spectra were recorded on a Hewlett-Packard 8453 diode array spectrometer using quartz cells (1.00 cm path length). Elemental analyses were performed by Canadian Microanalytical Services, Ltd., Delta, BC. Infrared Spectra were recorded on a 6021 GALAXY Series FT-IR.

Synthesis of (bme-dach)Ni·$2SO_2$, Ni-1′·$2SO_2$. A slurry of (bme-dach)Ni (107 mg, 387 mmol) in 15 mL of methanol was purged with gaseous SO_2 to yield a bright red precipitate. The solid was collected on a glass frit and dried under a stream of SO_2. Yield: 132 mg, 84.2%. Similarly, **Ni-1′·$2SO_2$** may be prepared in CH_3CN from which ruby red crystals of X-ray quality were obtained by slow diffusion of SO_2-saturated ether vapor, maintaining an atmosphere of SO_2. IR ν(SO) (KBr): 1229 and 1079 cm^{-1}. Vis-UV(acetonitrile), nm (ϵ = $M^{-1}cm^{-1}$): 356 (18 000). Elemental Anal. calcd (found) for $NiC_9H_{18}N_2S_4O_4$: C, 26.7 (27.0); N, 6.91 (6.93); H, 4.48 (4.54).

The **Ni-1′·**SO_2 adduct was obtained from overnight vacuum (0.7 Torr) of completely dried, powdered **Ni-1′·**$2SO_2$. The resulting red-orange, air-stable **Ni-1′·SO_2** powder had ν(SO) IR bands identical to those of its precursor. Elemental Anal. calcd (found) for $NiC_9H_{18}N_2S_3O_2$: C, 31.7 (31.6); N, 8.21 (8.18); H, 5.32 (5.25).

X-ray Crystal Structure Determination. Low-temperature (110 K) X-ray diffraction data were collected on a Bruker SMART CCD-based diffractometer (Mo Kα radiation, λ = 0.71073 Å) and covered a hemisphere of space upon combining three sets of exposures. The space group was determined based on systematic absences and intensity statistics using the SMART[13] program for data collection and cell refinement. Raw data frame integration was performed with SAINT+.[14] Other programs used included SHELXS-86 (Sheldrick)[15] for structure solution, SHELXL-97 (Sheldrick)[16] for structure refinement and SHELXTL-Plus, version 5.1 or later (Bruker),[17] for molecular graphics and preparation of material for

(11) Smee, J. J.; Miller, M. L.; Grapperhaus, C. A.; Reibenspies, J. H.; Darensbourg, M. Y. *Inorg. Chem.* **2001**, *40*, 3601−3605.
(12) Mills, D. K.; Font, I.; Farmer, P. J.; Hsiao, Y.; Tuntulani, T.; Buonomo, R. M.; Goodman, D. C.; Musie, G.; Grapperhaus, C. A.; Maguire, M. J.; Lai, C.; Hatley, M. L.; Smee, J. J.; Bellefeuille, J. A.; Darensbourg, M. Y. *Inorg. Synth.* **1998**, *32*, 89−98.
(13) SMART 1000 CCD. Bruker Analytical X-ray Systems: Madison, WI, 1999.
(14) SAINT-Plus, version 6.02 or later. Bruker: Madison, WI, 1999.
(15) Sheldrick, George. *SHELXS-86: Program for Crystal Structure Solution*; Institüt für Anorganische Chemie der Universität: Gottingen, Germany, 1986.
(16) Sheldrick, George. *SHELXL-97: Program for Crystal Structure Refinement*; Institüt für Anorganische Chemie der Universität: Gottingen, Germany, 1997.
(17) SHELXTL, version 5.1 or later. Bruker: Madison, WI, 1998.

publication. The structure was solved by direct methods. Anisotropic displacement parameters were determined for all non-hydrogen atoms. Hydrogen atoms were added at idealized positions and refined with fixed isotropic displacement parameters equal to 1.2 times the isotropic displacement parameters of the atoms to which they were attached.

TGA Sample Preparation. Thermogravimetric analyses were performed on an Instrument Specialist Inc. TGA 1000. Samples weighing between 3 and 5 mg were loaded onto a platinum weighing boat and heated at a rate of 5 °C per minute over a temperature range of 20−300 °C. Samples had to be completely dry as any residual solvent would result in larger temperature ranges of SO_2 loss.

Determination of SO_2 Detection Levels. The limits of visual SO_2 detection levels were determined according to a method described by Eller and Kubas.[9] Test strips were made by pouring a slurry of 9 mg of (bme-dach)Ni or **Ni-1′** in 2 mL of acetonitrile onto a piece of filter paper. The poor solubility of **Ni-1′** hampered even impregnation of the filter paper. The test strips were suspended in a rubber-septum-sealed 1-L flask, the volume of which had been precisely determined. Volumes of SO_2 on the order of 25−100 μL were added using a gastight syringe; the flask was swirled and color changes (tan to yellow-orange) were noted after 2 to 3 min. The greater solubility of (bme-daco)Ni, **Ni-1**, in CH_3CN produced more consistency in filter paper coverage, and color changes (purple to yellow-orange) of the test strips were more distinct than those seen for **Ni-1′.** Activity in test strips was restored by warming them in a 120° oven for 1 min. and "wetting" them with CH_3CN. Both the **Ni-1** and the **Ni-1′** strips were cycled for up to 10 times with no noticeable degradation.

Results and Discussion

Synthesis and Isolation. Synthesis of the SO_2 adduct resulted from bubbling SO_2 gas through slurries of **Ni-1′** in acetonitrile or methanol. In acetonitrile, the complex was rapidly solubilized as SO_2 was taken up and transformed into a dark red solution; ether vapor diffusion produced pure crystalline material. In CH_3OH, where solubility of the adduct is very low, the tan slurry readily changed into a yellow-orange solution upon exposure to SO_2 and a bright red precipitate formed. The product, **Ni-1′**·$2SO_2$, was collected on a glass frit under a stream of SO_2; filtration open to air resulted in loss of SO_2. Loss of an equivalent of SO_2 also occurs when powdered **Ni-1′**·$2SO_2$ is placed under vacuum overnight. A crystal of this **Ni-1′**·SO_2 adduct suitable for X-ray diffraction was not obtained, however elemental and thermal gravimetric analyses confirmed the formulation.

Molecular Structure by X-ray Diffraction Analysis. The large ruby red crystals obtained from vapor diffusion of SO_2-purged ether into an acetonitrile solution of **Ni-1′**·$2SO_2$ were found to be in the *P*2(1)/*c* space group. Table 1 lists the cell parameters and data collection parameters; Table 2 contains selected metric data for the molecular structure. Views of the structure are found in Figures 2−4, and a packing diagram is provided in the Supporting Information. Figure 2 presents the thermal ellipsoid plot of the fundamental unit of **Ni-1′**·$2SO_2$, and an atom labeling scheme. The coordination geometry and metrics within the N_2S_2Ni unit are largely unaltered from those of the SO_2-free **Ni-1′**. As has been noted in all bme-dach derivatives, the restriction of the seven-membered diazacycle produces a pinched N−Ni−N angle of 83°, with a concomitant opening of the S−Ni−S angle to 94.2°, maintaining rigorous planarity. In comparison, the analogous angles in the bme-daco derivatives are 90°, and a tetrahedral twist of 13−15° is observed.[11] The absorption of two equivalents of SO_2 by **Ni-1′** results in an increase in crystal density by 9.9%; in contrast, the crystal density for **Ni-1** increases by 4.2% upon SO_2 uptake, forming **Ni-1**·SO_2.[6,18]

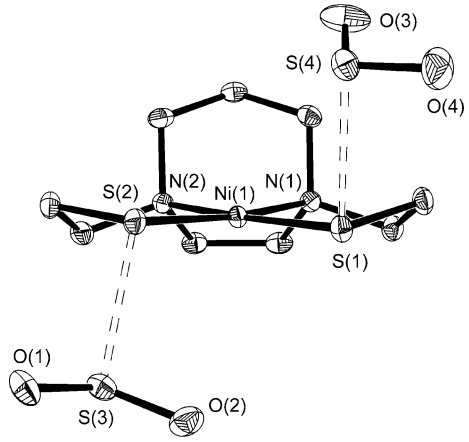

Figure 2. Molecular structure of (bme-dach)Ni·$2SO_2$ shown as thermal ellipsoids at 50%.

Table 1. Crystallographic Data for **Ni-1′**·$2SO_2$

	Ni-1′·$2SO_2$
formula	$C_9H_{18}N_2NiS_2$·$2SO_2$
molecular weight	405.20
temperature (°C)	−173.15
wavelength (Å)	0.71073
Z	4
D calcd (g cm^{-3})	1.807
μ (cm^{-1})	18.75
crystal system	monoclinic
space group	$P2_1/c$
unit cell	
a (Å)	10.308(4)
b (Å)	13.334(5)
c (Å)	10.842(4)
β (°)	91.963(6)
V (Å^3)	1489.3(10)
GOF	1.051
R_1,[a] wR_2[b] [$I > 2s(I)$]	0.0207, 0.0511
R_1,[a] wR_2[b] (all data)	0.0228, 0.0520

[a] $R_1 = \sum||F_o| - |F_c||/SF_o$. [b] $wR_2 = [\sum[w(F_o^2 - F_c^2)^2]/\sum w(F_o^2)^2]^{1/2}$.

Table 2. Selected Distances (Å) and Angles (°) for **Ni-1′**·$2SO_2$

distances		angles	
Ni(1)−N(1)	1.9190(18)	N(1)−Ni(1)−N(2)	82.87(7)
Ni(1)−N(2)	1.9216(18)	S(1)−Ni(1)−S(2)	94.25(3)
Ni(1)−S(1)	2.1585(9)	N(1)−Ni(1)−S(1)	91.54(6)
Ni(1)−S(2)	2.1607(9)	C(6)−N(1)−C(2)	110.63(17)
N(1)−C(6)	1.500(3)	C(6)−N(1)−C(3)	110.05(16)
S(1)−C(1)	1.824(2)	C(6)−N(1)−Ni(1)	108.00(13)
S(1)−S(4)	2.660(1)	C(3)−N(1)−Ni(1)	105.23(13)
S(1′)−S(4)	3.450(1)	Ni(1)−S(2)−S(3)	105.21(3)
S(2)−S(3)	2.5567(11)	O(2)−S(3)−O(1)	113.04(9)
S(3)−O(2)	1.4566(17)	O(2)−S(3)−S(2)	100.53(7)
S(3)−O(1)	1.4564(17)	O(1)−S(3)−S(2)	99.04(7)
S(4)−O(4)	1.4412(17)	O(4)−S(4)−O(3)	114.22(11)
S(4)−O(3)	1.4463(16)	N(1)−C(6)−C(7)	109.51(18)

(18) Darensbourg, M. Y.; Mills, D. K.; Reibenspies, J. H. *Inorg. Chem.* **1990**, *29*, 4364−4366.

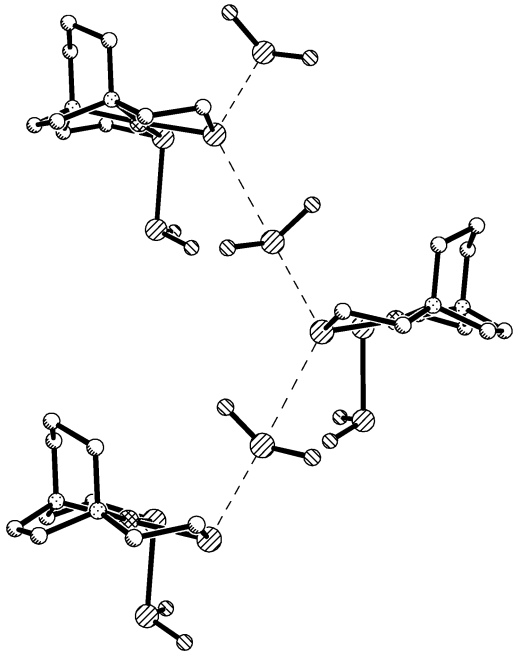

Figure 3. Extended chain SO_2 interaction showing the bridging SO_2 with hatched lines and showing the terminal interaction SO_2 with a solid line.

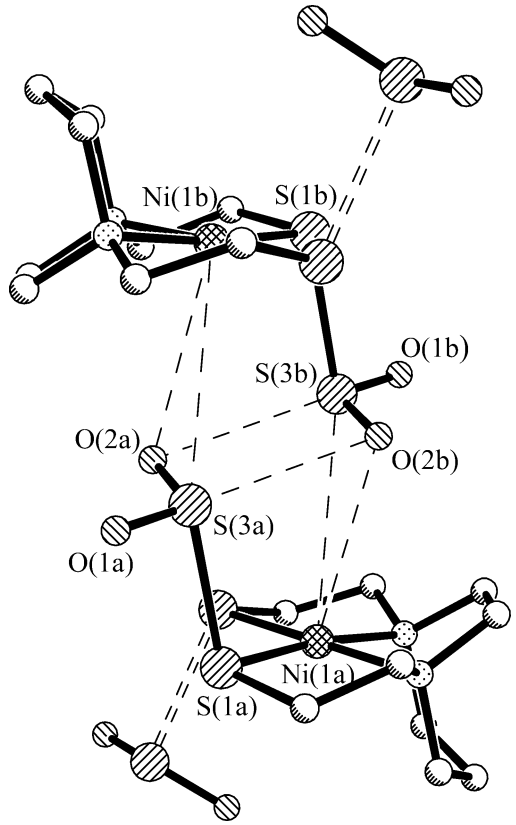

Figure 4. View of the dimeric unit emphasizing the S(1)−S(3) close contact. Double hatch lines identify bridging SO_2 of extended chain interaction. Selected distances: Ni(1a)−O(2b), 3.38 Å; Ni(1a)−S(3b), 3.72 Å; S(1a)−S(3a), 2.56 Å; and S(3b)−O(2a), 3.22 Å.

Figure 2 shows two SO_2 molecules are each attached through their sulfurs to individual thiolate sulfurs on opposite sides of the N_2S_2Ni plane at distances of 2.557(1) and 2.660(1) Å. The latter is involved in an extended zigzag chain structure, bridging to an adjacent **Ni-1′** through a 3.450 Å $S_{(thiolate)}-S_{(SO_2)}$ long-range interaction shown in Figure 3. This distance is within the van der Waals radii of S- - -S (3.6 Å). The zigzag chain is largely as found in the previously published structures of the **Ni-1**·SO_2 and **Pd-1**·SO_2 adducts.[6,7]

The second SO_2 molecule is not a part of the extended chain structure and has the shorter S··SO_2 distance of 2.557(1) Å. Figure 4 focuses on its involvement in dimeric units in which the "terminal" SO_2 molecules are caught between two N_2S_2Ni units that are related by an inversion center. Thus, these SO_2 molecules are mutually oriented toward the sterically less encumbered $N(CH_2)_2N$ side of the N_2S_2Ni resulting in what would appear to be long range η^2−(S═O) interactions to the adjacent nickel. On the other hand, the Ni- -$S_{(SO_2)}$ and Ni- -$O_{(SO_2)}$ distances of the apparent η^2−(S═O) interaction are 3.72 and 3.38 Å, respectively, and are 0.3 Å longer than the van der Waals contacts of 3.4 and 3.1 Å expected for Ni- -S and Ni- -O, respectively.[19] Hence, although appealing, the significance of this orientation in terms of orbital overlap and chemical bonds is suspect. The two entrained SO_2 molecules form a planar S_2O_2 parallelogram, and the pyramidality of the SO_2 within the adduct bonding arrangement results in the remaining oxygens being above and below the S_2O_2 plane by 0.279 Å.

It should be noted that the principal interactions in the **Ni-1′**·$2SO_2$, are the $S_{(thiolate)}$- -$S_{(SO_2)}$ Lewis base/Lewis acid interactions at 2.6 Å. This results in pyramidal SO_2 units both in the SO_2 that participates in the extended chain as well as that which is involved in the terminal $S_{(thiolate)}$- -$S_{(SO_2)}$ interaction.

Spectral Characteristics. Sulfur dioxide adducts of the square planar N_2S_2M complexes (M = Ni, Pd) have ν(SO) in the characteristic ranges of 1325−1210 and 1145−1060 cm^{-1},[20] as compared to 1340 and 1150 cm^{-1} of free SO_2 in acetonitrile. Earlier we and others noted an inverse correlation between the band positions and the stability of the metallo−thiolate−SO_2 adducts.[1,7] An increase in nucleophilicity of the thiolate sulfur Lewis base donor, which increases the adduct stability, results in a greater repulsion between the sulfur lone pair electrons of SO_2 and the π-electron density of the S═O bond. The resulting lower SO bond order accounts for the negative shift in ν(SO) values. Although the two types of SO_2 molecules in the **Ni-1′**·$2SO_2$ adduct should display individual sym and asym ν(SO) vibrational modes for a total of four bands in this region, only two strong bands are observed (KBr pellet, 1229 and 1079 cm^{-1}, assigned as asym and sym vibrational modes, respectively). The similarity to the **Ni-1**·SO_2 adduct (1217, 1075 cm^{-1}), and consistency with the powder diffraction studies, suggests these strong absorptions are due to the SO_2 molecules of the extended chain. As the characteristic ν(SO) IR bands derived from the bis adduct, **Ni-1′**·$2SO_2$, are slightly higher than those recorded for **Ni-1**·SO_2 (1217, 1075 cm^{-1}), a weaker SO_2 adduct is to be expected for the former. We

(19) Huheey, J. E. *Inorganic Chemistry: Principles of Structure and Reactivity:* Harper & Row: New York, 1972; pp 184−185.
(20) Ryan, R. R.; Kubas, D. C.; Eller, P. G. *Struct. Bonding* **1981**, *46*, 47−100.

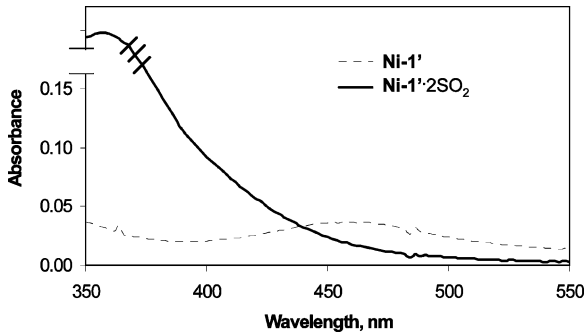

Figure 5. UV−vis spectral overlay of **Ni-1′** and its SO_2 adduct in CH_3CN solution; positions of λ_{max} and extinction coefficients are given in text.

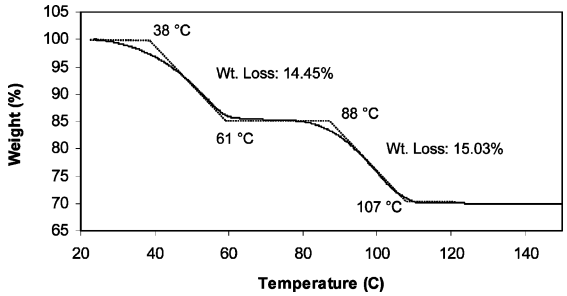

Figure 6. Thermogravimetric analysis plot of **Ni-1′**·$2SO_2$.

assume the lack of the second set of absorptions from the bis SO_2 adduct arises from pellet preparation.

In CH_3CN solution the UV−vis spectrum of the poorly soluble, tan (bme-dach)Ni finds a d−d transition at 460 nm and $\epsilon = 290\ M^{-1}cm^{-1}$. Upon exposure to SO_2 the tan slurry becomes a bright red solution with a charge-transfer band at 358 nm ($18\ 200\ M^{-1}cm^{-1}$) in CH_3CN. Figure 5 shows an overlay of the electronic spectra of **Ni-1′** and the **Ni-1′**·$2SO_2$ adduct. The large difference in molar absorptivity of the distinguishing absorptions of the two complexes did not permit comparisons of solutions of equal concentrations. Characterization below 330 nm is inconclusive due to the two intense charge-transfer bands of SO_2 at 212 and 280 nm.

Reversibility of SO_2 Binding and Thermogravimetric Analysis. The reversibility of SO_2 binding to **Ni-1′**·$2SO_2$ was qualitatively observed by gentle heating of powdered adducts whereupon SO_2 release was noted by smell and by color change of the residue. The bright red adduct reformed from the tan solid on exposure to SO_2. This reformation was nearly quantitative as indicated by similar TGA plots of the **Ni-1′**·$2SO_2$ adduct isolated from the methanol precipitation techniques versus the solid phase reaction. Figure 6 shows the thermogravimetric pyrolysis curve which clearly indicates the desorption of two equivalents of SO_2. The expected percent weight loss of each SO_2 in **Ni-1′**·$2SO_2$ is 15.8%. The observed weight loss in the temperature range from 38 to 60 °C was 14.5%. A second event occurred in the range of 80 to 110 °C with a 15.0% weight loss. The higher temperature range (97−133 °C) required to drive off the SO_2 in **Ni-1**·SO_2 is consistent with the analysis of ν(SO) infrared data described above. (N. B., the observed temperature range is narrower than that previously published, apparently due to sample dryness.)[7]

As evidenced by thermogravimetric and elemental analysis one equivalent of SO_2 is lost from **Ni-1′**·$2SO_2$ upon overnight vacuum at 0.7 Torr. The pyrolysis curve of the **Ni-1′**·SO_2, thus obtained, shows one equivalent of SO_2 (17.4% mass loss found; 18.8% expected) desorbs in the range of 85−110 °C. Analysis of crystalline and powdered forms of the adduct resulted in similar TGA pyrolysis curves and elemental analyses.

Detection Levels of SO_2. Visual detection of SO_2 uptake by solid **Ni-1′** on impregnated paper test strips, where a color change from yellow to yellow-orange occurs, could be distinguished at levels as low as 100 ppm of SO_2 in air. Increasing SO_2 concentrations to above 300 ppm produced more significant color changes. Increases in intensity of color with higher levels of SO_2 provided a crude measure of SO_2 concentration. The SO_2 could be easily removed from the **Ni-1′**·$2SO_2$ indicating strips by gently heating the strips (such as placing them in a 120° drying oven) or placing them in a stream of dinitrogen. At least 10 repeated cycles of adding and removing SO_2 did not diminish the effectiveness of the strips, even when run in air.

The greater effectiveness of **Ni-1** compared to **Ni-1′** is a result of better test strip coverage and a greater difference in color between the bright purple free dithiolate and the red-orange SO_2 adduct which permitted visual detection at the 25 ppm level.

Reactivity with Oxygen: Sulfate-Forming Reactivity. As previously mentioned, **Ni-1**·SO_2 reacts with O_2 to form dissulfide, sulfate, and the blood-red trimetallic $(\mathbf{Ni\text{-}1})_2Ni^{2+}$ species, Scheme 1. In contrast, when the bright red/orange acetonitrile solution of **Ni-1′**·$2SO_2$, in the presence of excess SO_2, was vigorously purged with O_2 for 15 min in a Schlenk flask, no change in color to the dark red of the trimetallic $(\mathbf{Ni\text{-}1'})_2Ni^{2+}$ species was observed.[21] Reversal of the order of gas addition was similarly unproductive, nor was there any indication of reactivity with dioxygen in the absence of SO_2. Sulfur dioxide was then bubbled through the O_2-saturated solution producing a clear, bright red solution indicative of SO_2 adduct formation. Extended periods in the presence of O_2 had no effect on the **Ni-1′** complex or the **Ni-1′**·$2SO_2$ adduct.

Summary and Comments

The salient features of this study are as follows. Sulfur dioxide uptake by the dithiolato nickel complex, **Ni-1′**, results in a crystalline material in which thiolate-sulfur to SO_2-sulfur interactions are well-defined by X-ray crystallography, ν-(SO) IR spectroscopy, and thermal gravimetric analysis. In this manner, the **Ni-1′**·$2SO_2$ adduct is placed in the series of thiolate bound compounds[7] according to the stability of the adducts as follows: **Ni-1**·SO_2 > **Ni-1′**·$2SO_2$ > **Ni-1***·SO_2 > **Ni-2**·SO_2, where **Ni-2** is the phosphinothiolate $(Ph_2PCH_2CH_2S)_2Ni$, and **Ni-1*** is the sterically hindered N,N′-bis(2-mercapto-2-methylpropyl)-1,5-diazacyclooctane)nickel(II) or (bme*-daco)Ni.[7]

(21) Golden, M. L.; Jeffery, S.; Reibenspies, J. H.; Darensbourg, M. Y. *Eur. J. Inorg. Chem.* **2004**, 231−236.

The many intermolecular interactions revealed in the crystal packing diagram of **Ni-1′**·2SO_2 are interpreted as the reason that **Ni-1′** is able to take up two equivalents of SO_2, whereas **Ni-1** absorbs only one. The space made available by the contracted diazaheptacycle (as compared to the diazaoctacycle) framework readily permits the second SO_2 to bind to the remaining thiolate. Although positioning of the terminal SO_2 unit between two N_2S_2Ni planes could be solely the result of spatial availability and optimal crystal packing, it is tempting to interpret the orientation of S═O side-on to nickel as a long range η^2-SO interaction. Nevertheless, both SO_2 molecules of the **Ni-1′**·2SO_2 adduct are removable by heating the solid or by purging solutions with argon or air. Also, the **Ni-1**·SO_2 adduct releases its SO_2 in the solid phase by heating or in solution upon purging with argon.

Because of more dramatic color changes upon uptake of SO_2 by **Ni-1** vs **Ni-1′**, the visual detection level of the former is 25 ppm SO_2 in air, while that of the latter is 100 ppm. The test strips were reactivated upon heating and rendered more sensitive by wetting with acetonitrile. The sensitivity of **Ni-1′** as an SO_2 detector is comparable to that of the $Cu(PR_3)_n(SR')$ complexes published by Kubas and Eller,[9] whereas that of **Ni-1** appears to be significantly better. Notably, the thiolate S-based SO_2 sensors derived from both copper(I) and nickel(II) thiolates appear to be more sensitive than the platinum(II)-based sensor reported by van Koten.[3] Exact side-by-side comparisons of **Ni-1** and **Ni-1′** with van Koten's and Kubas's SO_2 sensor molecules were not carried out.

Extended exposure of **Ni-1**·SO_2 to air results in a loss of the sensing capabilities of **Ni-1** due to the sulfate forming reaction described in Scheme 1; however, O_2 reactivity is sufficiently slow so as to minimally interfere with the SO_2 sensing application on fresh samples. Indicator strips containing **Ni-1** were regenerated with gentle heating at least 10 times over the course of several hours without loss of activity. The **Ni-1′** and **Ni-1′**·2SO_2 compounds are stable in air and were extensively recycled.

Admittedly, the design for technical application of our nickel dithiolate SO_2 sensing materials is crude. Even so, the visual detection is apparently the best of those chemical-based SO_2 sensors recently reported. One would expect that a judicious selection of a film for compound impregnation, coupled with development of a UV−vis spectroscopic-sensing technique, might greatly enhance detection limits. Nevertheless, the possibility of a visual "litmus test" based on an inexpensive base metal complex which is selective for SO_2 is an appealing prospect.

Acknowledgment. We acknowledge the financial support of the National Science Foundation (Grants CHE 01-11629 to MYD for this work and CHE 98-07975 for the purchase of X-ray equipment) and contributions from the Robert A. Welch Foundation.

Supporting Information Available: Thermal gravimetric analysis plots, packing diagram, tables of data for the subject compounds (pdf). Complete details of the X-ray diffraction studies for **Ni-1′**·2SO_2 (cif). This material is available free of charge via the Internet at http://pubs.acs.org.

IC049387N